Desalination 600 (2025) 118517

Contents lists available at ScienceDirect

Desalination

journal homepage: www.elsevier.com/locate/desal

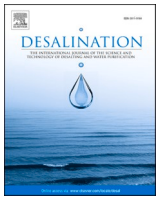

Sodium metasilicate sol-gel draw solution for seawater desalination and supplementing nutrients to soil

Tayma Kazwini [a], Ali Altaee [a,*], Ibrar Ibrar [a], Firas Alkadour [b], Alaa H. Hawari [b], John Zhou [a], Lilyan Alsaka [a]

[a] Centre for Green Technology, School of Civil and Environmental Engineering, the University of Technology Sydney, 15 Broadway, NSW 2007, Australia
[b] Department of Civil and Environmental Engineering, College of Engineering, Qatar University, PO Box 2713, Doha, Qatar

HIGHLIGHTS

- Sodium metasilicate was used as a draw solution for seawater desalination by forward osmosis.
- Reaction products of Na_2SiO_3 with HNO_3 are sol-gel of silicic acid and Na_2NO_3 plant nutrients.
- A water flux of 23.24 LMH was achieved with 1 M sol-gel DS and DI water feed solution.
- CTA membrane rejected 99 % of silica resulting in 8.85 g/Lm^2 RSF only for 1 M sol-gel.
- The specific energy consumption was as low as 0.00717 kWh/m^3 for 1 M sol-gel DS.

GRAPHICAL ABSTRACT

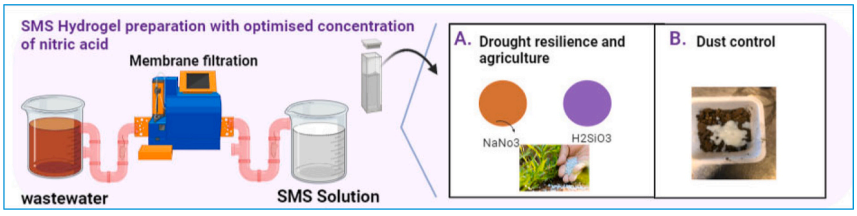

ARTICLE INFO

Keywords:
Forward osmosis
Hydrogel
Desalination
Draw solution
Membranes

ABSTRACT

A novel sol-gel using sodium metasilicate (SMS) was used as a draw solution (DS) in the forward osmosis (FO) to provide nutrients to soil and plants without a regeneration step. SMS sol-gel has an osmotic pressure of 55 bar and 73.4 bar for 0.75 M and 1 M of SMS, respectively, which is higher than 1 M NaCl (48.9 bar). To test the novelty of the SMS sol-gel as DS, two concentrations of 0.75 M and 1 M were tested against DI water and 0.5 M NaCl feed solution (FS), and 1 M of SMS for real seawater at 35 g/L. A commercial cellulose triacetate (CTA) membrane was used, where experimental results showed SMS at 1 M using DI water as FS at active layer draw solution (ALDS) membrane orientation had a 42 % recovery rate, compared to active layer feed solution (ALFS) at 36 % recovery. The highest average flux achieved was 23.24 LMH with DI water as FS, using 1 M SMS sol-gel as DS at ALDS. Whereas using seawater at ALDS had a 23.5 % recovery and ALFS had a 15.2 % recovery. Testing seawater at ALDS with three 24-h cycles had 55.8 %, 45.4 %, and 32.9 % recovery for the first, second, and third cycles, respectively. There was a 99 % rejection of silicon and sodium ions for both SMS concentrations. The specific energy consumption was lowest at 0.00717 kWh/m^3 in the first 24-h cycle of seawater as FS.

* Corresponding author.
E-mail address: ali.altaee@uts.edu.au (A. Altaee).

https://doi.org/10.1016/j.desal.2024.118517
Received 15 October 2024; Received in revised form 20 December 2024; Accepted 29 December 2024
Available online 30 December 2024

1. Introduction

Rising water scarcity and climate change pose a growing concern in multiple geographic areas worldwide, with primary impacts observed in Northern Africa, Southeast Asia, and the Middle East [1,2]. With increasing population, improper land use and management, and extreme weather conditions, the search for a clean water source continues to be one of the most significant challenges of the 21st century. Industries and their land use and waste disposal measures also have an impact on water scarcity and nutrient depletion of aquatic and land habitats [3]. The agricultural industry consumes over 70 % of the world's water sources for irrigation [4,5]. The reliance on precipitation can negatively impact the yield of crops produced, most specifically during extreme drought conditions, as it affects the concentration and infiltration of soils, ultimately influencing land management [6]. With higher water shortages being experienced, harvesting capabilities have been reduced, and land degradation has increased, eventually decreasing the biodiversity of the soil [7]. In addition to water scarcity, climate change has a severe impact on the environment, presented in desertification and dust storms, degrading arable land quality, where 250 million people worldwide live in severe arid/semi-arid regions [8,9]. The scourge of dust storms, fuelled by desertification and land degradation, further compounds environmental woes, impacting human health and ecosystem stability. Physical, chemical, and biological methods were suggested for land restoration and dust control [10–12].

Chemical agents, such as calcium chloride, magnesium chloride, sodium lignosulfonate, super-adsorbent polymers, and sodium metasilicate (SMS), were suggested for dust control and land restoration [13,14]. Sodium metasilicate, an adhesive compound widely used in industries, is alkaline, colourless, non-flammable, and last for extended periods of storage [15]. It has multiple applications in soil stabilization/solidification, nutrient supply to plants, and dust control [11,16,17]. In soil solidification, SMS is mixed with a metal salt or acid to form a sol-gel. Sodium metasilicate is applicable for sandy soil stabilization, forming gelatinous metal silicates [11]. In addition to soil treatment, studies demonstrated that sodium silicate improves the germination and growth of wheat [16]. Another study by Zhou et al. (2018) suggested that sodium metasilicate improved cucumber growth and resistance to pathogens [17]. However, the high pH levels of SMS need to be mitigated to avoid negatively impacting the surrounding environment [18]. The wide range of sodium metasilicate applications for land restoration, dust palliative, and improving plant germination and growth offer opportunities for further investigation as a draw solution in the forward osmosis process for dilution and membrane purification technologies. In the latter application, SMS will be the draw solution, while seawater is the feed solution for SMS dilution.

SMS can be prepared in situ when freshwater is available for the applications mentioned above. Unfortunately, a water source of low salinity is not easily accessible in arid or remote mining regions. Accordingly, a membrane technology could be adapted for desalination and wastewater treatment for freshwater supply. Forward osmosis (FO) technology has been investigated for the past two decades, including for seawater mining to extract minerals [19], urban runoff [20], and leachate wastewater treatment [21], and has increasing potential for commercial applications. Compared to reverse osmosis (RO) membrane technologies with increasing maintenance and operation costs, FO is an alternative technology that can perform quality water treatment without hydraulic pressure and reduce fouling tendency and, thus, maintenance and energy costs [22–24]. The FO depends on osmotic pressure between concentrated and diluted solutions to drive the filtration process. Once the permeate water dilutes the draw solution, it can undergo further regeneration treatment or be used directly [8,25,26]. The diluted SMS draw solution could be used directly without the regeneration process. By omitting the regeneration process, the cost of the FO for processing the SMS will be significantly reduced.

Although hydrogel or solution-gel (sol-gel) draw solution has been investigated in the past, there are a few studies in this field. Li et al. (2011) investigated two ionic and two non-ionic polymer hydrogels as draw solutions in forward osmosis. All four of the conducted experiments produced an initial water flux of <1.2 LMH [27]. Another study by Li et al. (2011) further investigated composite polymer hydrogels against pure polymer hydrogels, once again resulting in an initial water flux of <1.5 LMH [28].

This study proposed SMS as a novel draw solution in the FO process to produce a hydrogel as a sol-gel for multiple applications, including dust suppression, a source for nitrogen fertilizer, land restoration, and soil improvement. The SMS sol-gel will be diluted in the FO process, omitting the regeneration process for direct application on soil for plant growth, land restoration, and dust control. The research questions are: i) Does SMS sol-gel generate enough water flux in the FO process? ii) Is the FO membrane fouling reversible when seawater is the feed solution, and iii) what is the specific power consumption for SMS dilution? Three types of water sources were investigated as feed solutions, including deionized water (DI water), sodium chloride (NaCl) solution, and finally, real seawater. A commercial cellulose triacetate (CTA) membrane (Sterlitech, USA) was applied in the FO process. The experimental work studied the impact of membrane orientation, SMS concentration, and feed salinity on the water flux.

2. Methodology

2.1. FO membrane characteristics

A commercial cellulose triacetate (CTA) membrane, FTSH2O™ (Sterlitech, USA), was implemented for this investigation. Table 1 shows the data on the membrane characteristics obtained from the manufacturer Sterlitech. Before use, the CTA membrane was immersed in DI water to ensure complete wetting. Furthermore, before commencing the experiments, the membrane was washed with DI water for 30 min to remove any additives from the surface. The contact angle of the active and support layers of the membrane was measured by the sessile drop method (Biolin Scientific ThetaLite 100). Malvern Panalytical instrument (Malvern Zetasizer) measured the zeta potential of the FO membrane. To determine the pore radius of the CTA membrane, the porosity (φ) was calculated using the wet and dry weights of the membrane, using gravimetric measurements as per eq. 1 [29]:

$$\varphi = \frac{\frac{w_1 - w_2}{\rho_w}}{\frac{w_1 - w_2}{\rho_w} + \frac{w_2}{\rho_p}} \quad (1)$$

Where w_1 is the wet weight of the membrane in grams, w_2 is the dry weight of the membrane in grams, and ρ_w is the density of water (1.00 g/cm^3), and ρ_p is the density of the polymer. Following this, the average pore radius (R_m) was also calculated using the Guerout-Elford-Ferry Eq. [30]:

$$R_m = \frac{\sqrt{(2.90 - 1.75\varphi)8\hbar T J_w}}{\varphi P A} \quad (2)$$

Table 1
CTA membrane characteristics.

Parameters	$FTSH_2O$ CTA Flat Sheet membrane
Feed temperature (°C)	Maximum = 50
pH range	3–7
Chlorine tolerance	Maximum = 2 ppm
Transmembrane Pressure	Minimum = 5 psi
Contact angle active layer (°)	68.1 ± 1
Contact angle support layer (°)	60.2 ± 0.5
Zeta Potential (mV)	−12.8 ± 1.18
Average pore radius at pH 5 (nm)	27.94
Average pore radius at pH 7 (nm)	28.2
Average pore radius at pH 9 (nm)	30.70

Where h is water viscosity (Pa s), Jw is water flux per unit time, P is operational pressure (0.1 MPA), A is effective membrane area, T is the membrane thickness, and φ is membrane porosity.

2.2. Sodium metasilicate hydrogel preparation

A 300 mL DI water was added to different weights of sodium metasilicate in a 1 L beaker with continuous stirring to produce a homogeneous solution. A 45 g and 61 g of SMS were mixed with DI water to produce 0.75 M and 1 M SMS solution concentrations. The reaction was conducted in a fume hood, and nitric acid was gradually added to the SMS solution to neutralize the alkaline pH. The SMS solution turned to a milky colour just below pH 11. An additional 200 mL DI water was added gradually to the SMS solution under continuous stirring until the solution attained a pH of 7–8. It was envisioned that the SMS reaction with nitric acid (70 % concentration) would reduce the solution pH to about pH 7 to 8 to produce sodium nitrate ($NaNO_3$) and metasilicic acid (H_2SiO_3) as follows:

$$2HNO_3 + Na_2SiO_3 \rightarrow 2NaNO_3 + H_2SiO_3 \quad (3)$$

Sodium nitrate is a fertilizer and source of nitrogen for plants' growth, while silicic acid hydrogel is a soil stabilizer [31,32]. The reaction products can be used to provide essential nutrients to plants and dust control.

2.3. Forward osmosis system

The experiment setup will consist of a forward osmosis (FO) laboratory-scale crossflow filtration, the CF042A-FO Cell, manufactured by Sterlitech (United States) with a 42 cm^2 (0.0042 m^2) active membrane area. The CTA membrane was placed in the FO-Cell, where the feed solution flowed across the membrane into the draw solution. Both feed and draw solutions were circulated at 2 L per minute (LPM) using a WT3000-1JA Micro Gear Pump by Longer Pump for each solution. This circulation was consistent throughout the experiment to ensure no impact on the results. A flow meter from Blue-White Industries Ltd. F-550 model F-55375 L was used, one on the draw side of the cell and the other on the feed side of the cell. The pH of the feed and draw solution was measured using the Jenco (Australia) Vision Plus pH 6810, ensuring pH stability. Fig. 1 shows a schematic diagram of the FO unit. The feed solution was placed on an EK-15KL compact bench scale, connected to a laptop with a data logging system, RsWeight, to measure the changing mass of the solution as water moved from the feed solution compartment to the draw solution compartment.

As part of the experimentation, two concentrations, 0.75 M and 1 M of sodium metasilicate-based draw solution, were tested, both active-layer facing feed solution (ALFS) and active-layer facing draw solution (ALDS). For all FO experiments, the DS beaker was placed on a magnetic stirrer, ensuring the solution's homogeneousness. The tests were conducted at laboratory room temperatures, which are approximately 25 °C. The electronic scale will be connected to a laptop during the FO process, automatically measuring the feed solution's mass change. The feed and draw solution samples were characterized using ICP-MS analysis. Furthermore, SEM and EDX were used to investigate the membrane fouling, and FT-IR was used to investigate the functional groups of the membrane.

The permeation mass was recorded in 15-min intervals and converted to water flux using the following formula:

$$J_w = \frac{\Delta m}{\rho . A . t} \quad (4)$$

Where J_w is water flux (LMH), Δm is the mass difference (kg), ρ is the density (kg/L), A is membrane area (m^2), and t is time (h).

The reverse salt flux (J_s), which is the back-and-forth diffusion of salts across the membrane, can be calculated by:

$$J_s = \frac{C_1 m_1 - C_0 m_0}{At} \quad (5)$$

J_s is the salt flux (g/m^2h), C_1m_1 is feed concentration and mass after time (t), and C_0m_0 is feed concentration and mass at a time (0). The concentration of salts in the feed solution was measured using a conductivity meter.

The rejection rate was calculated to investigate the sodium (Na) and silica (Si) levels present when DI water is the feed solution and silica when NaCl is used as the feed solution.

$$R = \left(1 - \frac{C_p}{C_f}\right) \times 100\% \quad (6)$$

C_p (mg/L) is the permeate concentration, and C_f (mg/L) is the solute concentration.

As it is a novel draw solution, the recovery rate was investigated to

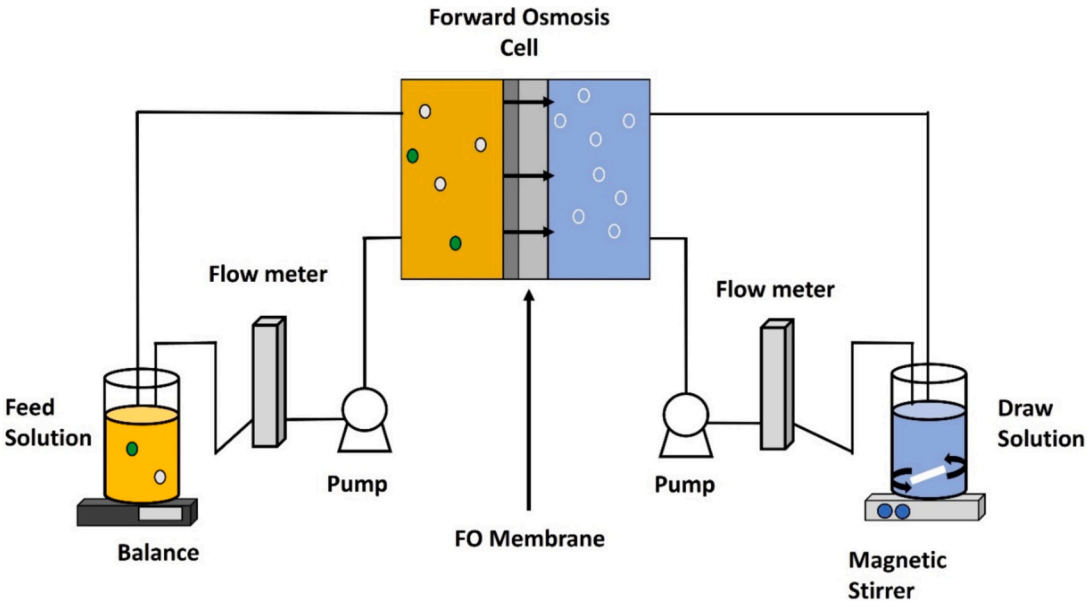

Fig. 1. Forward osmosis system setup using a flat sheet FTSH2O membrane in the Sterlitech CF042A-FO Cell.

understand the mechanism of SMS and how much permeate is recovered, using the following formula:

$$Recovery = \frac{Q_p}{Q_f} * 100\% \quad (7)$$

Q_p is the permeate flow (m^3/h), and Q_f is the feed flow rate (m^3/h).

The following formula calculates the specific power consumption (E_s – kWh/m^3) of the FO system:

$$E_{s-FO} = \frac{P_f Q_f + P_d Q_d}{\eta . Q_p} \quad (8)$$

Where P_f is the feed pressure (bar), and P_d draw solution feed pressure (bar), the Q_f and Q_d for this experiment, both the feed pressure and draw solution pressure were maintained at 2 LPM, η represents the pump efficiency (0.85), and Q_p is the permeate flow. The specific energy used for seawater as a feed solution was calculated.

Water flux recovery (FR) was calculated after each cycle using the expression below:

$$FR = \frac{J_1}{J_0} \times 100\% \quad (9)$$

J_0 represents the average flux from the first cycle, whereas J_1 represents the average flux taken from the second cycle.

2.4. Feed solution

For the feed solution, DI water was utilized to have a basis for the results and to understand the interactions of SMS sol-gel as a draw solute. The second part of the experiments used 0.5 M of NaCl solution as the feed solution to represent the average seawater total dissolved solids (TDS). Finally, real seawater was used as the feed solution in the final section of the experiments. Seawater was collected from the coastlines of Sydney, NSW. Table 2 shows the compositions of the collected seawater samples. This investigation used two SMS concentrations, 0.75 M and 1 M.

2.5. Hydrogel rheology and swelling properties

RheoCompass (Anton Parr, Australia) rotational rheometer was employed as the primary tool for characterization. The hydrogel samples comprising varying concentrations were subjected to rheological measurements to investigate the hydrogels' mechanical properties and viscoelastic behavior. Prior to testing, each sample underwent careful preparation, ensuring uniformity and consistency. The rheological measurements were conducted under specific conditions, and parameters such as viscosity and shear stress were determined to assess the structural and flow properties of the hydrogels. The RheoCompass software facilitated the interpretation of the rheological data, providing valuable insights into the performance and rheological characteristics of the SMS hydrogel at different concentrations. This methodology contributes to a comprehensive understanding of the hydrogel's mechanical behavior, essential for its potential applications in various fields.

The hydrogel water content and swelling are important characteristics that determine the hydrogel's water-holding capacity. Hydrogel specimens, each with a thickness of 2 cm, were utilized for water content and swelling tests, all conducted under neutral pH conditions. The hydrogel water uptake (WU) was calculated by drying hydrogel samples in an oven at 105 °C for 6 h, and the dry weight ($W_{driedhydrogel}$) was recorded. Post-drying, the pieces were immersed in DI water at room temperature for 24 h, and after removing excess moisture using blotting paper, the moist weight ($W_{moisthydrogel}$) was determined. The water uptake was then calculated using the following equation, with 5 samples tested and the average results reported.

$$Water\ uptake = \frac{W_{moisthydrogel} - W_{driedhydrogel}}{W_{moisthydrogel}} \quad (10)$$

Furthermore, the swelling degree of the hydrogel, indicative of its anti-swelling properties, was assessed. The initial weight of the hydrogel ($W_{initial}$) was recorded and placed in DI water for 2 h or a NaCl solution of varying concentrations. The final weight (W_{final}) was recorded, and the swelling degree (SD) was determined using the following equation.

$$SD = \left(W_{final} - W_{initial}\right) * W_{initial} * 100 \quad (11)$$

Brunauer-Emmett-Teller (BET) analysis was conducted on the hydrogel where nitrogen gas, acting as an absorbate, was used on 1 g of dried hydrogel and placed in a glass column. Following this, degas was carried out for 4 h. Pore size analyses were conducted on the samples for 4 h.

Table 2
Seawater composition and characteristics.

Ions/Parameters	Concentration	Ions/Parameters	Concentration
Ca^{2+} (mg/L)	605	Suspended Solids (mg/L)	0.48
Mg^{2+} (mg/L)	1519.3	TDS (mg/L)	34,566
Cl^- (mg/L)	8504	Conductivity (mS/cm)	49
Na^+ (mg/L)	12,526.7	pH	6.31
K^+ (mg/L)	558.2	Turbidity (NTU)	0.27
SO_4^- (mg/L)	2743.5		

2.6. Hydrogel and membrane morphological characterization

Dried samples of SMS hydrogel, featuring concentrations ranging from 0.75 M to 1 M, underwent a systematic characterization using advanced microscopy techniques. Firstly, for Scanning Electron Microscopy (SEM), the dried hydrogel samples were meticulously prepared by oven-drying at 105 °C for 6 h. These dried samples were mounted on aluminum stubs, coated with a thin layer of gold/palladium, and examined using a high-resolution scanning electron microscope (Zeiss, Sydney, Australia) to unravel detailed surface morphology. Simultaneously, Energy Dispersive X-ray Spectroscopy (EDX) was employed alongside SEM to explore the elemental composition using the same instrument. The SEM instrument, equipped with an EDX detector, facilitated elemental mapping and qualitative analysis, providing insights into the distribution of elements within the hydrogel structure. Fourier Transform Infrared Spectroscopy (FT-IR) was also conducted to delve into the molecular structure. The preparation of hydrogel was similar to using the SEM/EDX instruments. Dried hydrogel specimens were ground into fine powder and analyzed using a Fourier transform infrared spectrometer, unveiling characteristic peaks and molecular interactions indicative of the hydrogel's functional groups. Brunauer-Emmett-Teller (BET) analysis was also conducted on the hydrogel where nitrogen gas, acting as an absorbate, was used on 1 g of dried hydrogel and placed in a glass column. Following this, degas was carried out for 4 h. Pore size analyses were conducted on the samples for 4 h.

The contact angle of the used membranes was measured to gain insights into the surface wettability and hydrophilicity of the membrane after it had been used with SMS hydrogel as the draw solution. Water contact angles were determined using the Biolin Scientific ThetaLite 100 measurement system and a sessile-drop method. Each sample underwent measurements at a minimum of three different locations, and the average water contact angle, along with an associated error value, was reported as the final result.

3. Results and discussion

3.1. SMS hydrogel characterization

The SMS hydrogel was subjected to several tests to investigate its properties. Two Hydrogel samples were produced, one at 0.75 M and the second at 1 M SMS concentration. The tests conducted included BET

analysis, rheology tests to test the viscosity of the hydrogel, FT-IR of dried hydrogel, contact angle of the hydrogel, water content analysis, swelling, and SEM imaging.

3.1.1. Rheology

Hydrogels are viscoelastic materials and have the combined characteristics of solids and liquids. The viscosity of the SMS hydrogel was measured at 1 M concentration. The temperature was maintained at a constant 25 °C. Fig. 2a illustrates the shear rate against the viscosity (Pa). As can be seen from Fig. 2a, viscosity decreases as the shear rate increases, defining the hydrogel as a shear-thinning viscous capacity. The shear-thinning aspect of SMS hydrogel is classified within the non-Newtonian fluids. As a polymer with crosslink bonds, the SMS hydrogel structure stretches and realigns with moving discs as the shear increases, reducing viscosity. As a result, this realignment of the hydrogel structure causes an increase in porosity and breakdown of molecular interactions. Kestin et al. (1981) investigated the viscosity of sodium chloride aqueous solution with temperatures ranging from 20 to 150 °C and various pressures. The average viscosity was 973.2 mPa at 25 °C for 1 M of sodium chloride [33]. Compared to sodium chloride, the SMS solution's average viscosity of the peak from where the shear stress and viscosity graphs meet is approximately 5984 mPa·S, proving it has a very high viscosity and increases with the SMS concentration in the solution. Additionally, as will be seen from the FT-IR analysis of the SMS hydrogel, the hydroxyl groups, most specifically from the metasilicic acid, increase the intermolecular attractive forces, increasing the hydrogel's viscosity.

In Fig. 2a, the graph shows the relationship between the shear rate and the shear stress applied to the hydrogel. The shear stress peaks at approximately 80 Pa and drops steadily within the plastic or permanent deformation region, implying that the SMS hydrogel has the highest strength at 80 Pa. The hydrogel reaches a fracture point on larger strains, ultimately losing its strength, and deformation or degradation occurs. The SMS hydrogel is physical, meaning that when the sodium metasilicate and nitric acid combine to make sodium nitrate and metasilicic acid, non-covalent bonds link them. Regarding the viscous behavior of the hydrogel, after deformation, the SMS hydrogel can realign and come back together. The non-covalent bonds can degrade under stress yet conveniently retain their properties, and any changes are dependent on the environment, such as the pH and temperature [34]. Although the SMS hydrogel does not have a strengthened covalent crosslink, its ability to transform with environmental stimuli and revert to its strengths and capabilities without impeding its structure is a novel strength to be utilized within the FO system. The hydrogel, if it retains its structural integrity, can withstand more substantial dilution without compromising its porous properties. This characteristic would be helpful when testing the diluted draw solution on the soil's water-holding abilities.

3.1.2. FT-IR analysis

FT-IR was used to examine the functional groups of the dried SMS hydrogel. A 1 M SMS hydrogel solution was prepared, dried, and pulverized. Three different measurements were taken of the powder, and an average was formed to produce the graph in Fig. 2b. The graph shows several dips at either end of the wavenumbers. Between 3000 and 3708 cm^{-1}, a broad and sharp dip appears within the O—H stretching functional group. The O—H bonds are from the metasilicic acid, implying that hydroxyl is readily available. The intermolecular attractions of the O—H group readily attach to other hydrogen atoms in water, making it hydrophilic. Another dip that can be seen is between 1565 and 1753 cm^{-1}, where the peak is at 1646 cm^{-1} and lies within the C═O stretching functional group. Another dip is between 1261 and 1472 cm^{-1}, with a peak of approximately 1370 cm^{-1}. From the FTIR reference table, the functional group is O—H bending. Another large dip on the graph is between 847 and 1261 cm^{-1}, both broad stretch and strong peak, sitting at around 1040 cm^{-1}. The dip resides within the S═O stretching functional group, resulting from the silicic acid formed when mixing nitric acid and sodium metasilicate. Like other hydrogels, the SMS hydrogel can hold water due to the hydrophilic moieties of its hydroxyl functional groups and attach to other water molecules while keeping its structure intact. Additionally, between 566 and 847 cm^{-1} ranges, there is a Si—O symmetric stretching group, as well as between 400 and 500 cm^{-1}, there is a prominent peak which is associated with Si-O-Si bending vibration and is associated with the polymerization of the complex silicate structure [35].

3.1.3. Density, swelling, water content, and BET

The mechanical changes of a hydrogel can be related to its swelling, deswelling, and water content properties. For example, adding nitric acid to the SMS solution to stabilize the pH of the solution releases the silica from within the crosslink interaction of the polymer, affecting the hydrogel's mechanical strength [36]. When looking at a polymerized hydrogel for agricultural applications, the porosity and permeability of the hydrogel are essential to investigate.

Regarding the density calculation, the method used was a 25 mL volumetric flask for 0.75 M and 1 M SMS hydrogel. The density for 0.75 M and 1 M was 1.0592 g/m^3 and 1.1084 g/m^3, respectively. The density of the hydrogel is altered depending on the concentration of SMS, pH, and amount of nitric acid added to the solution. SMS hydrogel's density is higher than water's, causing it to sink at the bottom of the beaker (Fig. A1, Appendix). When observing the swelling behavior of the SMS solution, it was found to shrink rather than swell because of the phenomena of syneresis. Adding nitric acid releases the silicon from the sodium silicate and impacts its structure by reducing the porosity and making it harder [36,37]. The higher density suggests that it is suitable for water retention properties, which in irrigation applications implies the reduction of the frequency of irrigation. In terms of the specific

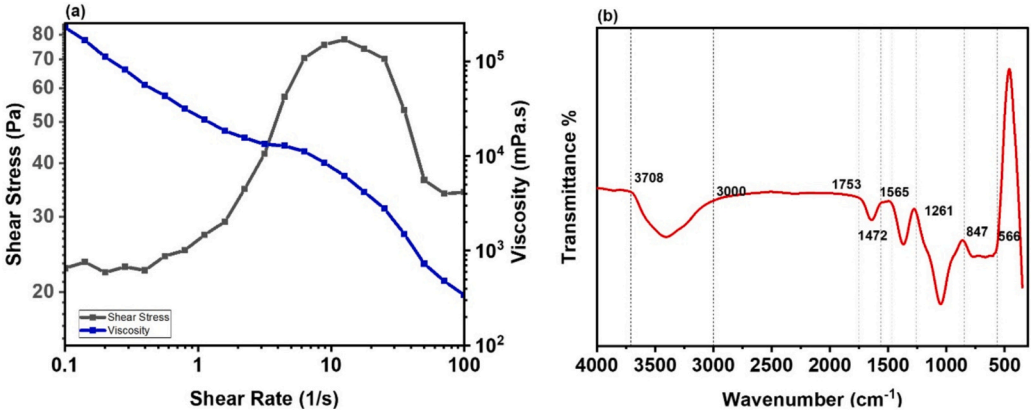

Fig. 2. (a) Shear rate against viscosity and shear stress of SMS hydrogel, (b) FT-IR of SMS hydrogel.

volume, being <1 m^3/g means that the hydrogel cannot retain water as well as other hydrogels; however, by reducing the SMS concentration, the specific volume increases, which improves water retention properties.

For the moisture content, 1 M SMS hydrogel was placed on a centrifuge at 2000 RPM for 2 min to remove excess water. The hydrogel was then placed on a petri dish in the oven at 105 °C for 2 h until completely dry. The calculated moisture content was 36 %, signifying the hydrogel's porous nature and ability to hold water. BET analysis was undertaken to determine the surface area and pore size of the SMS hydrogel. With a pore diameter of 4.75 nm, the SMS hydrogel can be classified as a macroporous material holding vast amounts of water. The hydrogel pore volume and pore diameter are 0.06 cc/g and 13.8 m^2/g, respectively. The tiny hydrogel's pores and surface area explain the 36 % water content. A smaller surface area can limit the amount of water that can be absorbed or held.

3.2. *Water flux*

Water flux provides insight into the viability of using the SMS draw solution in the FO process. The water flux was measured with sodium metasilicate (SMS) sol-gel as a draw solution and DI water, 0.5 M NaCl, and seawater feed solutions. The CTA membrane was positioned at the active layer facing the feed solution (ALFS) and the active layer facing

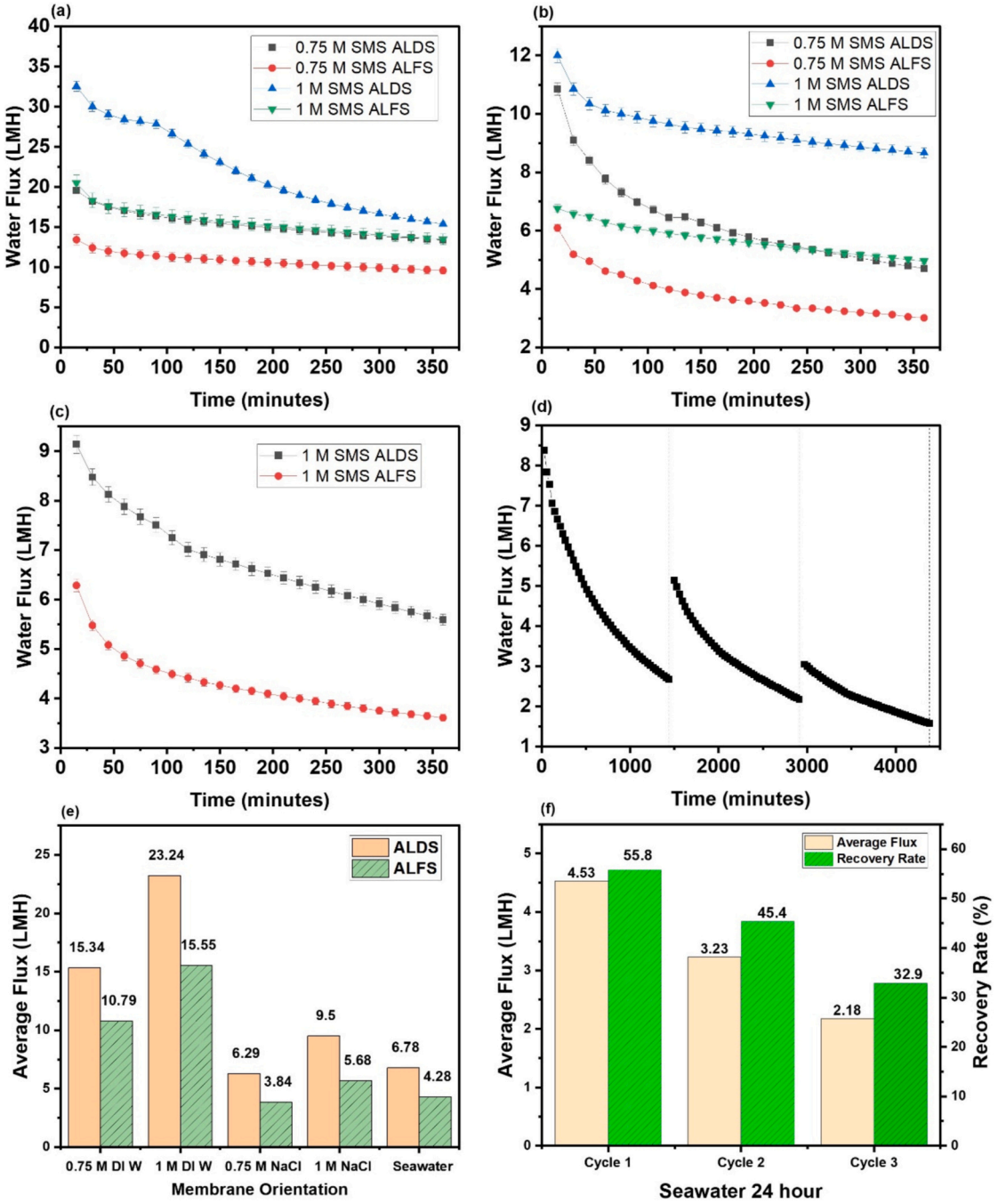

Fig. 3. Water flux for both membrane orientations at ALDS and ALFS, (a) DI Water as FS using 0.75 M & 1 M SMS concentrations, (b) 0.5 M NaCl as FS using 0.75 M & 1 M SMS concentrations, (c) seawater as FS using 1 M SMS concentrations, (d) seawater as FS for 3 × 24-h cycles, (e) average flux, (f) average flux and recovery rate for seawater for 3 × 24-h cycles.

the draw solution (ALDS) to evaluate the impact of membrane orientation on the water flux. The experiments were conducted for 6 h at each membrane orientation for two SMS concentrations, i.e., 0.75 M and 1 M, to study the impact of draw solution concentration on the water flux. Two feed solutions, DI water and NaCl, were used for each membrane orientation and 0.75 M and 1 M SMS concentration. For all experiments, the flow rate of the feed and draw solutions was maintained at 2 LPM, representing a crossflow velocity of 0.36 cm sec^{-1}. Furthermore, the temperature of the draw and feed solution was maintained at 25 °C.

Fig. 3a shows the water flux for 0.75 M and 1 M SMS concentration using DI water as feed solution for both membrane orientations. With ALDS at 0.75 M SMS-DI water, the initial and final water flux was 19.52 LMH and 13.38 LMH, indicating a 31.4 % water flux decline in water flux in 6 h. With ALFS at 0.75 M SMS-DI water, the initial water flux was 7.33 LMH, and the final water flux was 5.25 LMH, resulting in a 28.6 % water flux decline. In comparison, water flux decline was faster in the ALDS direction due to the greater water flux. For ALDS with 1 M SMS-DI water, the initial water flux was 32.52 LMH, and the final water flux was 15.37 LMH, showing a 52.7 % decline in the water flux after 6 h. For ALFS with 1 M SMS-DI water, the initial water flux was 20.48 LMH and decreased to 13.47 LMH, resulting in a 34.2 % water flux decline.

While a higher water flux was achieved at 1 M SMS-ALDS, the overall water flux decline throughout the experiment was significantly higher than the 0.75 M SMS. The 1 M SMS produced a 2.3 times greater water flux than the 0.75 M SMS with DI water feed solution. Appendix A1 substantiates that the larger osmotic pressure of 1 M SMS (73.36 bar) compared to 0.75 M SMS (55.02 bar) generated more water flux, causing rapid draw solution dilution by the high permeate flux. In contrast, a lower water flux was achieved in the ALFS than in the ALDS because of the intensive ICP that cannot be easily mitigated [38]. Increasing the SMS concentration by 33 %, from 0.75 M to 1 M, more than doubled the initial water flux.

The impact of the feed solution on the water flux was evaluated using NaCl feed solution. Fig. 3b shows the water flux for 0.5 M NaCl as a feed concentration resembling seawater using 0.75 M and 1 M SMS for both membrane orientations. For ALDS with 0.75 M SMS, the initial water flux was 10.86 LMH, and the final was 4.71 LMH, resulting in a 56.7 % water flux decline. However, for ALFS with 0.75 M SMS, the initial water flux was 6.10 LMH and decreased to 3.02 LMH at the end of the FO test, resulting in a 50.5 % decline in water flux. In the case of ALDS with 1 M SMS, the initial and final water flux was 12 LMH and 8.67 LMH, respectively, resulting in a 27.8 % water flux decline, while ALFS's initial and final water flux was 6.76 LMH and 4.96 LMH, respectively, indicating a 26.6 % water flux decline. As per Appendix A1, the osmotic pressure of 0.75 M and 1 M SMS is 55.02 and 73.36 bar, respectively, compared to 24.46 bar for 0.5 M sodium chloride. In practice, water flux decreases with increasing the feed solution due to the decreased osmotic driving force and intensive concentrative CP.

Compared to FO tests with DI water, there was a higher decline in water flux using NaCl as FS, primarily due to i) the higher initial water flux when DI water is the FS that resulted in a rapid DS dilution and ii) severe CP in the FO tests with 0.5 M NaCl FS, resulting in reduced water flux. The water flux in the FO tests with DI water FS was almost three times greater than the NaCl FS, accelerating the DS dilution and rapidly decreasing the osmotic pressure driving force.

According to Table 3, SMS hydrogel's high density (1.1084 g/m3 for 1 M) and viscosity ($3.2*10^3$ mPa.s) slow its diffusion from the bulk solution to the membrane surface, especially in the ALFS mode. Thus, the internal CP intensifies in the ALFS orientation compared to the ALDS. For example, the results in Fig. 3a and b show that the initial water flux with 0.75 M SMS-ALDS is substantially greater than in 0.75 M SMS-ALFS, and it is almost equal to that in 1 M SMS-ALFS despite its higher osmotic pressure (Appendix A1). The reason for this is due to the difficulties for the SMS hydrogel to penetrate through the support membrane layer in the ALFS mode besides the effect of internal CP. Therefore, operating the FO in the ALDS yields better water flux, considering the FS quality responsible for membrane fouling.

Table 3
Fluid Properties of SMS Hydrogel.

Properties of SMS hydrogel	SMS 0.75 M	SMS 1 M
Density, (g/m^3)	1.0592	1.1084
Specific Volume (m^3/g)	0.944	0.9022
Specific weight (N/m^3)	10.39	10.87

In comparison to the study of SMS sol-gel as DS, Idris et al. (2021) investigated various molarities of NaCl as DS. At 1 M NaCl, being the highest molarity tested, the water flux was approximately 8.5 LMH [39]. In comparison, at 0.75 M SMS, the water flux achieved was more than double the literature findings. Fig. 3e shows the average water flux for 0.75 M and 1 M SMS draw solutions in the FO operates in the ALDS and ALFS. As expected, the average water flux increased with the SMS draw solution's concentration. The average water flux for DI water feed solution tests was 23.24 LMH and 15.34 LMH for the 1 M and 0.75 M SMS in the ALDS. The corresponding water flux for 1 M and 0.75 M SMS in the ALFS was 15.55 LMH and 10.79 LMH. A slightly higher average water flux was achieved in the FO tests with 1 M SMS compared to the 0.75 M SMS DS due to the tangible water flux in the DI water tests and insignificant CP.

On the contrary, there was a considerable average water flux difference due to the SMS concentration increase in the FO tests with 0.5 M NaCl draw solution. There is a 51 % average water flux difference due to increasing the SMS concentration from 1 M to 0.75 M in the ALDS FO tests with NaCl feed solution. Looking at the effect of membrane orientation, specifically for NaCl as FS and 0.75 M SMS DS, there was an 18 % difference in average flux between ALDS to ALFS. Severe concentrative CP and slow diffusion of SMS sol-gel into the support membrane layer (in the ALFS) are the main reasons for the marginal difference in the average water flux of the FO tests with NaCl feed solution.

3.3. Reverse salt flux

The reverse salt flux (RSF), or reverse salt diffusion, is the diffusion of salts going back across the semi-permeable membrane from the draw solution into the feed solution compartments, most explicitly contributing to draw solution loss. Using DI water as the feed solution, a conductivity meter was used to measure the TDS of the feed solution throughout the experiments. The results found that the conductivity in the FS increased with time. As the SMS concentration increased from 0.75 M to 1 M, the J_s also increased (Fig. 4a). In ALDS tests, for example, RSF was 1.65 g/m^2h and 8.85 g/m^2h for 0.75 M and 1 M SMS draw solution concentrations. RSF was lower in the ALFS tests, 1.04 g/m^2h and 4.53 g/m^2h for 0.75 M and 1 M SMS, due to the impact of dilutive ICP, reducing the SMS concentration at the membrane surface. The larger molecular weight of SMS (122.06 g/mol) and high viscosity are accountable for the low RSF in the FO membrane compared to conventional draw solutions. A previous study by Yahia et al. 2024 revealed that the RSF for 1 M NaCl and $MgCl_2$ in the ALDS test was 22.56 g/m^2h and 12.30 g/m^2h, respectively [40]. Compared to this study, the RSF of 1 M SMS is much lower than for NaCl and $MgCl_2$ draw solutions, indicating a crucial advantage of SMS in the reduction of RSF in the FO process [41].

The Inductively Coupled Plasma-Mass Spectrometry (ICP-MS) was used to measure the concentration of sodium and silica in the feed solution (Fig. 4b). For 0.75 M SMS, the sodium concentration in the feed solution was 0.21 g/L and 0.15 g/L in ALDS and ALFS, where ALFS had only slightly lower sodium concentration due to the intensified ICP on the draw solution side. The sodium concentration increased to 0.64 g/L and 0.58 g/L in the ALDS and ALFS tests with 1 M SMS draw solution. In contrast, the silica concentration was 0.03 g/L in the ALFS with 0.75 M SMS test, while it was not detected in the ALDS tests. For 1 M SMS, the

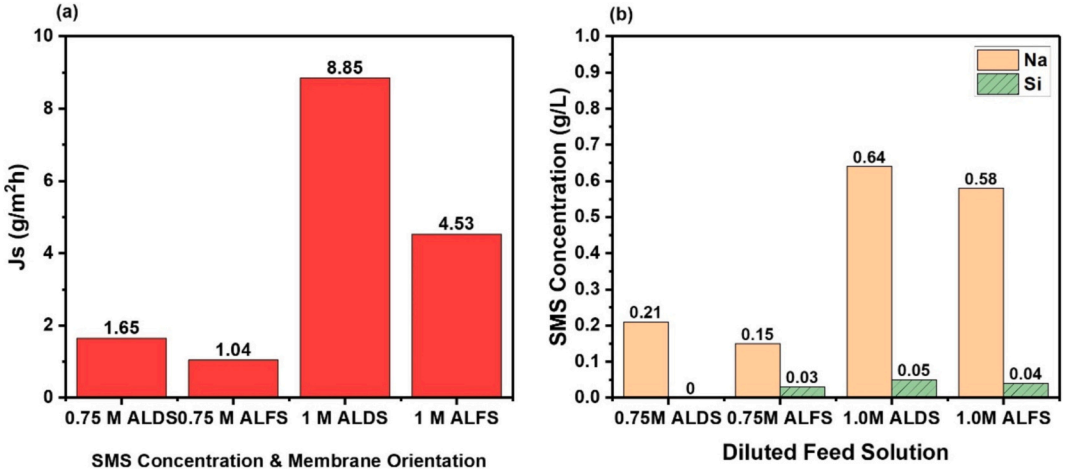

Fig. 4. a) Reverse Salt Flux (RSF) for DI Water as FS for both 0.75 M and 1 M SMS sol-gel at ALFS and ALDS membrane orientation, (b) sodium and silica rejection from the feed solution using DI water.

silica concentration subtly increased to 0.05 g/L and 0.04 g/L in the ALDS and ALFS, respectively. The CTA FO membrane exhibited over 99 % rejection of SMS in both membrane orientations.

3.4. Seawater feed solution

Seawater with 34.5 g/L concentration was used as the FS when investigating 1 M SMS sol-gel to generate enough osmotic pressure driving force for freshwater extraction. Initially, the FO membrane was tested for 6-h at both membrane directions, and the best performance membrane orientation was tested in three 24-h cycles, using DI water to clean both sides of the membrane between each cycle, and membrane fouling was monitored.

Fig. 3c shows the FO tests with 1 M SMS DS and seawater FS for the 6-h experiment. At ALDS, the initial water flux began at 9.14 LMH, decreased gradually, and reached 5.59 LMH after 6-h, resulting in a 38.8 % decline. However, at ALFS, the initial was 6.29 LMH, and the final water flux was 3.61 LMH, indicating a 42.6 % decline in water flux. The severe dilutive ICP was responsible for the steeper water flux decline in the ALFS test. There was a sharp drop in water flux over the first 30 min due to a combination of greater DS dilution and initial membrane fouling by the seawater. Fig. 3e shows the average water flux in the FO experiments, with the average water flux with seawater being lower than that for the 0.5 M NaCl FS due to the slight variation in the osmotic pressure driving force and probably membrane fouling by the seawater. Results show that an average water flux of 6.78 LMH and 4.28 LMH was achieved in the ALDS and ALFS FO tests with seawater feed solution and 1 M SMS draw solution compared to 9.5 LMH and 5.68 LMH for 0.5 M NaCl feed solution and 1 M SMS draw solution.

The 6-h 1 M SMS-seawater tests in the ALDS showed higher average water flux than at ALFS; therefore, three 24-h cycles were used at 1 M SMS-ALDS. Fig. 3d shows the performance of these cycles. DI water was used to clean the membrane for 60 min between the cycles to investigate if it was adequate for membrane cleaning and water flux recovery. The initial water flux of the first cycle was 8.38 LMH, and the final was 2.68 LMH, resulting in a 68 % water flux decline over 24 h. In the second cycle, the initial water flux was 5.14 LMH, and the final water flux was 2.18 LMH, resulting in a 57.6 % water flux decline. The third cycle achieved the lowest water flux, with an initial water flux of 3.05 LMH and a final water flux of 1.58 LMH, resulting in a 48.2 % decline. Individually, the water flux decline was 38.7 % and 40.7 % in the second and third cycles due to fouling materials build up on the membrane. The results indicate that membrane cleaning with DI water was ineffective, and there was an increase in fouling after each cycle. The average water flux in the first, second, and third filtration cycles was 4.53 LMH, 2.32 LMH, and 2.18 LMH, respectively, while the corresponding recovery rate was 55.8 %, 45.4 %, and 32.9 %, respectively (Fig. 3f). Membrane fouling was responsible for the reduction in water flux and the recovery rate in the consecutive filtration cycles.

The FR between the first and second cycles was 61 % and 59 % between the second and third cycles. Additionally, the average water flux of each cycle was reduced. The results indicate that the effect of fouling on the membrane increased when the experiment was extended from 6-h to 24-h, and fouling mitigation methods are required to retain the membrane's water flux. Additionally, results imply seawater pretreatment and/or cleaning methods should be investigated to combat the effects of fouling and ICP/ECP and see if this improves the water flux, rather than using DI water alone to clean the membrane between uses and cycles.

3.5. FT-IR, SEM/EDX, contact angle

The FT-IR analysis was conducted for the CTA membranes as follows: i) membrane 1 is for a pristine CTA membrane, ii) membrane 2 refers to seawater 6-h tests, and iii) membrane 3 is for 24-h tests with seawater. Fig. 5a shows the FT-IR for membrane 1, membrane 2, and membrane 3. There are several common peaks between 1314 and 1606 cm^{-1}; some are stretching and wide. Membrane 1 has a sharper peak at 1530 cm^{-1}, signifying strong N—O functional groups. All membranes have high transmittance of C═O stretching functional groups that do not seem to have been affected by the FO processes, between 1813 and 2809 cm^{-1}, specifically around the peak of 2300 cm^{-1} for membrane 3. The results show strong O═C═O stretching bonds, 2809 to 3018 cm^{-1}, and there is greater absorbance of N-H bonds for membrane 1. For membrane 2, the transmittance of the N-H bonds signifies stronger bonding between the nitrates and hydrogen molecules. There are minor wide peaks between 3018 and 3696 cm^{-1}, which is related to OH functional groups. The FT-IR analysis shows that the hydrogen and nitrate molecules created bonds and remained on the membrane after cleaning with DI water. When comparing this to membrane 3, there is not as much precision of the nitrates, most likely due to higher absorption rather than transmittance. Therefore, functional groups of note to mention are most specifically related to the N-H functional groups, showing stronger bonding between the nitrates from the sodium nitrate molecule and hydrogen from the membrane.

Fig. 5b and c show SEM images of fouled support and active layers for membrane 3 that experience considerable water flux decline after 24-h filtration. Fig. 5b shows moderate fouling on the active layer facing the draw solution. Although the membrane was flushed with DI water between each cycle, the SEM image shows some fouling, indicating the

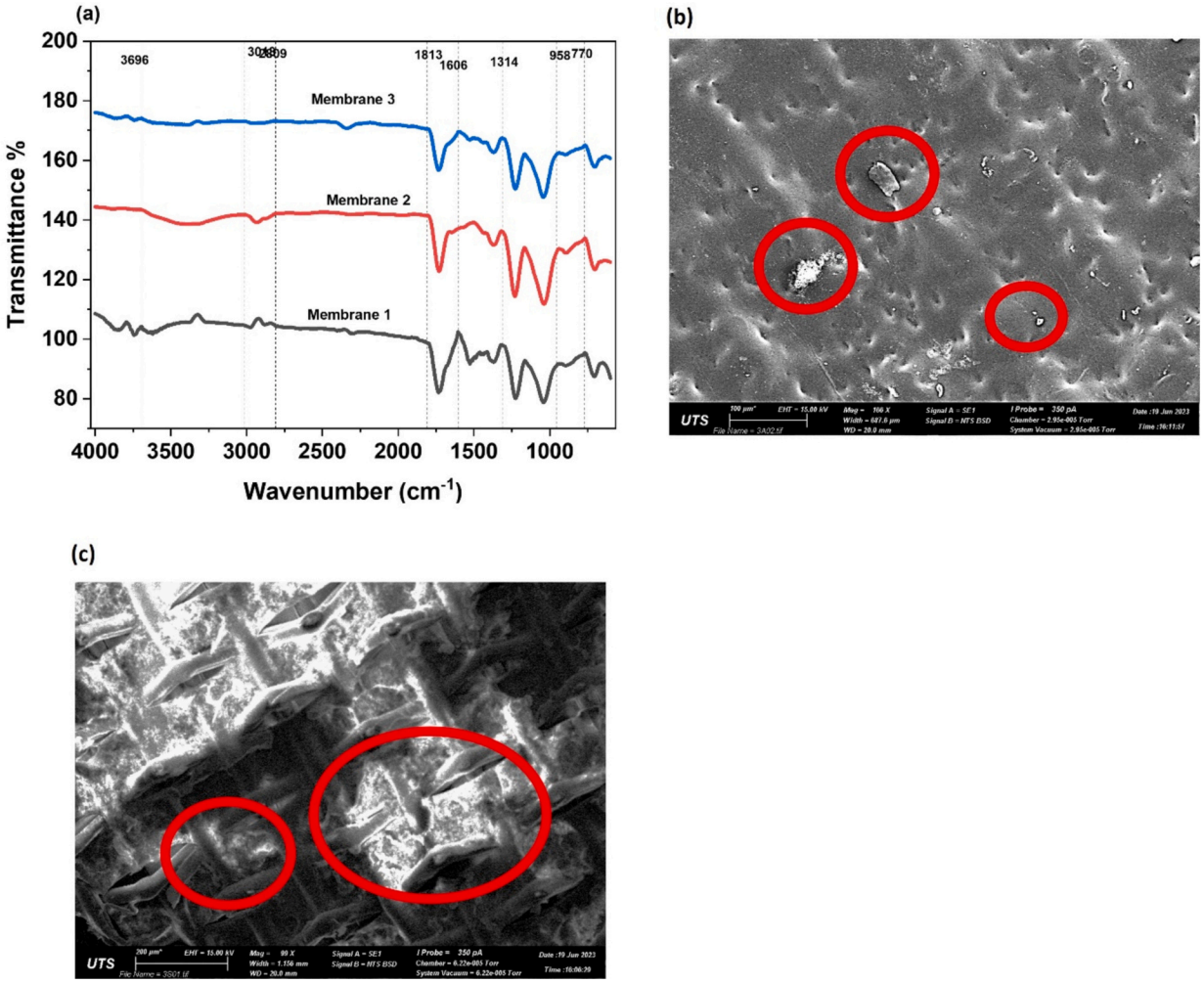

Fig. 5. (a) FT-IR of Membrane 1, 2, 3 (b) SEM of membrane 3 active layer (c) SEM of membrane 3 support layer.

ineffectiveness of DI water alone in cleaning to remove or reduce the fouling layer. Fig. 5c, however, shows the support layer of membrane 3 facing the feed solution. The layer of fouling materials on the support layer of the membranes also shows the implication of osmotic gradient reduction and compilation of organic and inorganic foulants from seawater feed. The diffusion of seawater ions from the feed to the draw compartment could be the reason for membrane fouling.

Energy-dispersive X-ray spectroscopy (EDX) was also carried out. A comparison of the elemental compositions of membranes 1 and 3 is presented in Table 4. The main changes from membranes 1 and 3 are the depletion of carbon, suggesting an increase in fouling on the membrane's surface, and the increase in oxygen for both active and support layers, implying the presence of some metal oxides on the membrane surface, which is particularly evident on the active layer of membrane 3 (Table 4). For example, the concentration of magnesium, manganese, and copper ions increased from 0.0 %, 0.01 %, and 0.02 % in the pristine membrane to 0.13 %, 0.02 %, and 0.3 % in membrane 3. These metal ions were diffused from the feed to the draw solution and resulted in membrane fouling. Notably, silicon fouling was not an issue although the active layer side of the membrane contacted with the SMS sol-gel. Silica concentration subtly increased from 0.01 % in the pristine membrane to 0.02 % in membrane 3.

Table 4
Elemental composition comparison between membrane 1 (pristine CTA membrane) and membrane 3 (using 3 cycles of 24 h with seawater as feed).

Elements	Membrane 1, support layer (wt%)	Membrane 3, support layer (wt%)	Membrane 1, active layer (wt%)	Membrane 3, active layer (wt%)
Carbon	49.8	45.02	48.46	46.12
Oxygen	49.3	52.62	51.05	51.68
Silicon	0.05	0.00	0.01	0.02
Sulfur	0.20	0.00	0.12	0.05
Chlorine	0.10	0.45	0.02	0.57
Calcium	0.11	0.00	0.02	0.01
Manganese	0	0.00	0.00	0.02
Iron	0	0.00	0.14	0.04
Copper	0.15	0.00	0.02	0.30
Sodium	0.12	1.15	0.11	1.10
Magnesium	0	0.00	0.01	0.13
Cadmium	0.15	0.00	0.02	0.00

The contact angle of the CTA membranes' active layer was measured after the filtration tests and compared with the pristine membrane contact angle in Table 1. The contact angle of Membrane 3 was reduced to 40.43°, which is a 42 % decrease. The decrease in the contact angle indicates the hydrophilicity of the membrane is increasing, probably due to the formation of metal oxides, such as magnesium oxide, on the active membrane layer of membrane 3. Table 4 shows an increase in magnesium, magnesium, and copper in the active layer of membrane 3. In effect, metal oxides enhance the water affinity of the membrane by introducing hydroxyl groups, enhancing water permeability.

3.6. Recovery rate and energy consumption

Table 5 shows the specific power consumption and recovery rate for

Table 5
Recovery rate and specific energy for all experiments with their corresponding SMS concentration and membrane orientation.

Feed Water Source	SMS Concentration	Membrane Orientation	Recovery Rate (%)	Specific Energy, Es (kWh/m^3)
DI Water	0.75 M	ALDS	33.7	0.00148
		ALFS	32.7	0.00153
	1 M	ALDS	42.0	0.00119
		ALFS	36.5	0.00137
0.5 M NaCl	0.75 M	ALDS	14.8	0.00422
		ALFS	9.5	0.00658
	1 M	ALDS	21.8	0.00229
		ALFS	15.6	0.00400
Seawater	1 M	ALDS	23.5	0.00355
		ALFS	15.2	0.00550
1st 24-h cycle Seawater	1 M	ALDS	55.8	0.00717
2nd 24-h cycle Seawater			45.4	0.00880
3rd 24-h cycle Seawater			32.9	0.01216

all FO experiments at various membrane orientations. As indicated in Table 5, for every feed solution and the SMS concentration, the ALDS membrane orientation has a consistently higher recovery rate than the ALFS membrane orientation. For example, at 0.75 M SMS-0.5 M NaCl draw solution and feed solution, there was a 56 % increase in the recovery rate for changing the membrane orientation from ALFS to ALDS. The FO tests with DI water feed solution accomplished higher recovery rates than those with 0.5 M NaCl and seawater due to the greater osmotic pressure and the negligible concentrative CP in the DI water tests. The recovery rate in the 1 M SMS-DI water test was almost twice that in the 1 M SMS-0.5 M NaCl or seawater, indicating the impact of feed salinity on the FO recovery rate.

The FO tests show an obvious increase in the specific energy requirements (E_s) in the FO tests that had a limited water flux. Table 5 shows that the FO tests with DI water feed solution induced the highest permeation flow (Q_p). All specific energy was below 0.02 $kWh/m^{3,}$ whereas RO uses up to 2 to 5 kWh/m^3 [42,43], showing a significant energy saving in FO systems compared to RO systems. Table 5 shows a slight increase in the energy requirements with an increase in feed salinity due to the reduced permeation flow. It is evident from Table 5 that the specific energy increased in ALFS due to the lower permeation flux and recovery rate compared to ALDS. Therefore, there is a correlation between the permeate and the specific energy. The 24-h seawater tests (ALDS), with a 55.8 % recovery rate, achieved 0.00717 kWh/m^3 E_s due to extended experimental time. The E_s increased to 0.00880 kWh/m^3 and 0.01216 kWh/m^3 in the second and third cycles, respectively, due to the lower water flux in these tests caused by membrane fouling. Previous studies have also linked FO energy consumption with fouling tendencies; the higher the fouling, the higher the energy consumption [44], and obviously a decline in permeate flux throughout the experiments. Overall, seawater would be an excellent potential feed solution with the SMS sol-gel as a draw solution, but it may need pretreatment to remove the fouling materials that are responsible for membrane fouling and or physical and or chemical cleaning between each cycle.

4. Conclusion

Sodium metasilicate (SMS)-based sol-gel draw solution was prepared from the reaction of SMS with nitric acid to produce silicic acid and sodium nitrate, which are essential nutrients for plants. Experiments revealed that SMS sol-gel possesses a considerable advantage, generating 15.34 LMH and 23.24 LMH average water flux for 0.75 M and 1 M SMS for DI water as feed, respectively, which is competitive to other hydrogel-based draw solutions such as conventional draw solutions such as NaCl and $MgCl_2$. The corresponding average water flux for 0.5 M NaCl was 6.29 LMH and 9.5 LMH for 0.75 M and 1 M NaCl draw solution, indicating the impact of feed TDS and CP on the FO performance. Although SMS exhibited a negligible RSF, the RSF was lower in the ALFS tests due to the dilutive ICP phenomenon and the relatively high SMS viscosity that impeded its diffusion into the support membrane layer. Generally, the ICP-MS test revealed that RFS was mainly the low molecular weight sodium ions that diffused from the draw to the feed solution. FO membrane fouling was detected in the 24-h filtration tests with seawater feed solution and 1 M SMS. In the 3 cycles of FO tests, the maximum water flux declined from 8.38 LMH in the first cycle to 3.05 LMH in the third cycle due to sodium or divalent ions such as calcium and magnesium. Future work should address membrane fouling by suggesting suitable cleaning methods and or seawater pretreatment to remove fouling materials. Overall, experiments demonstrated the feasibility of using SMS sol-gel as a draw solution in the FO process and its potential use for improving the soil water retention capacity and nutrient supply to plants.

CRediT authorship contribution statement

Tayma Kazwini: Investigation, Data curation, Investigation, Writing, Formal analysis, Visualization, and editing.

Ali Altaee: Conceptualization, Data curation, Investigation, Project admin, Writing, administration, Formal analysis, Visualization, Writing-review & editing, Supervision.

Ibrar Ibrar: Investigation, Data curation, Investigation, Formal analysis.

Firas Alkadour: Data Analysis, Writing - Review & Editing, Investigation.

Alaa Hawari: Project admin, Data curation, Writing.

John Zhou: Data curation, Supervision, Formal analysis, Writing - Review & Editing.

Lilyan Alsaka: Data curation, Investigation, Formal analysis.

Declaration of competing interest

The authors declare that they have no known competing financial interests or personal relationships that could have appeared to influence the work reported in this paper.

Acknowledgments

The author would like to acknowledge the scholarship awarded to Tayma Kazwini by the Australian Government under the Research Training Program scholarship.

This research is made possible by a food security research award (MME03-1015-210003) from the Qatar National Research Fund (QNRF) in partnership with the Ministry of Municipality.

Appendix A

A.1. Osmotic pressure

The osmotic pressure of Na_2SiO_3 was estimated using the Van't Hoff equation:

$\pi = iMRT$

Where π is the osmotic pressure, 'i' is Van't Hoff's factor, M is the molar solution concentration (mol/L), R is the ideal gas constant (0.08206 L atm mol^{-1}), and T is the temperature in Kelvin. For Na_2SiO_3, that value is 3. For temperature in Kelvin, the laboratory temperature was 25 °C, or 298 K. Two concentrations were used for sodium metasilicate, 0.75 M and 1 M. From Van't Hoff's equation, the osmotic pressure was 55.02 bar for 0.75 M SMS, 73.36 bar for 1 M SMS, and 48.91 bar for 1 M NaCl.

A.2. Swelling

A 50 mL vial consisting of 15 mL hydrogel, only undergone centrifuge to separate the gel from the solution, was used and mixed with 35 mL of 0.5 M NaCl. The solution and hydrogel were shaken and left at room temperature to investigate the swelling nature of the hydrogel. After 24 h, rather than swelling, the hydrogel was reduced by 33 % to 10 mL. A second and third 50 mL vials were used with 15 mL each of the SMS hydrogels; however, this time with 35 mL of DI water. The solution and hydrogel were shaken and left at room temperature for 24 h. After 24 h, one of the vials remained consistent at 15 mL, and the second was reduced slightly by 1 or 2 mL.

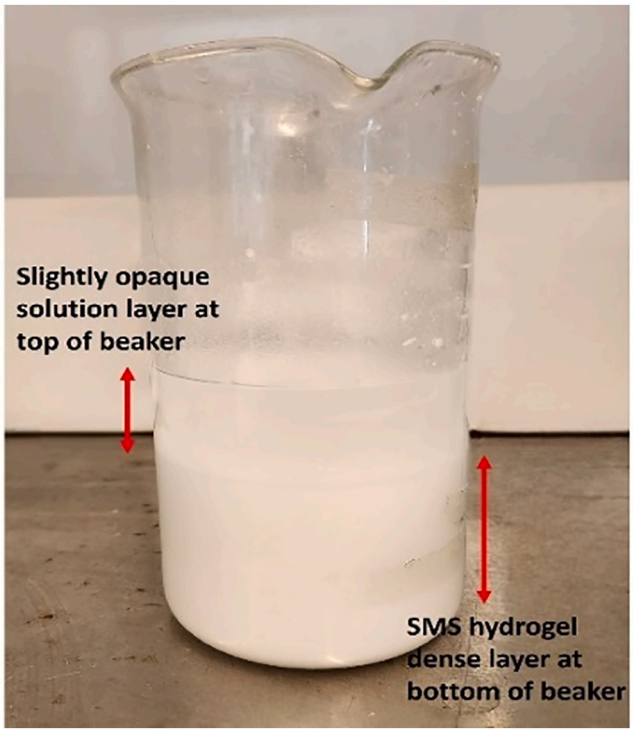

Fig. A1. SMS hydrogel layers, showing a high density of hydrogel at the bottom of the beaker.

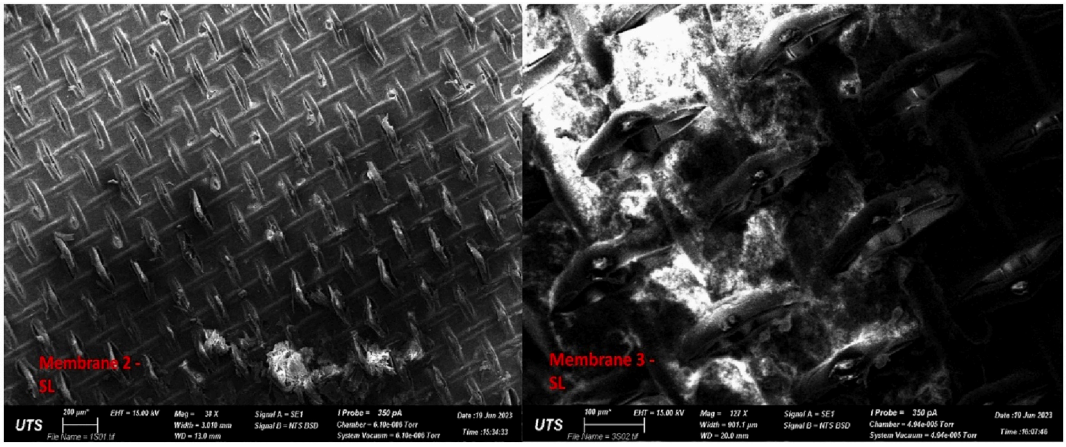

Fig. A2. SEM Images of the support layer of membranes 2 and 3.

A.3. Soil water retention capacity

Table A1
Water retention capacity of soil with and without sodium metasilicate treatment.

5 g soil +10 mL sodium metasilicate	Day 0	Day 1	Day 25	Weight Reduction (%)
Soil + Water	25.49	25.34	22.40	12.13
Soil +0.5 M	26.03	25.89	23.38	10.19
Soil +0.75 M	25.93	25.79	23.32	10.07

Data availability

Data will be made available on request.

References

[1] S.F. Anis, R. Hashaikeh, N.J.D. Hilal, Reverse osmosis pretreatment technologies and future trends: A comprehensive review, Desalination 452 (2019) 159–195, https://doi.org/10.1016/j.desal.2018.11.006.

[2] H. Shemer, S. Wald, R.J.M. Semiat, Challenges and solutions for global water scarcity, Membranes 13 (2023) 612, https://doi.org/10.3390/membranes13060612.

[3] P. Chowdhary, R.N. Bharagava, S. Mishra, N.J.E.C. Khan, W. Sustainable Development: Volume 1: Air, E. Resources, Role of industries in water scarcity and its adverse effects on environment and human health, Environmental Concerns and Sustainable Development, (2020) 235–256.doi:https://doi.org/10.1007/978-981-13-5889-0_12.

[4] R.L. McDaniel, C. Munster, J.J.T.o.t.A., Nielsen-gammon, crop and location specific agricultural drought quantification: part III. Forecasting water stress and yield trends, Trans. ASABE 60 (2017) 741–752, https://doi.org/10.13031/trans.11651.

[5] C. Ingrao, R. Strippoli, G. Lagioia, D.J.H. Huisingh, Water Scarcity in Agriculture: An Overview of Causes, Impacts and Approaches for Reducing the Risks, Heliyon, 2023.

[6] A. Calzadilla, K. Rehdanz, R. Betts, P. Falloon, A. Wiltshire, R.S.J.C.c., Tol, climate change impacts on global agriculture, Clim. Chang. 120 (2013) 357–374, https://doi.org/10.1007/s10584-013-0822-4.

[7] M.S. Habibullah, B.H. Din, S.-H. Tan, H.J.E.S. Zahid, P. Research, Impact of climate change on biodiversity loss: global evidence, Environ. Sci. Pollut. Res. 29 (2022) 1073–1086, https://doi.org/10.1007/s11356-021-15702-8.

[8] J. Duan, E. Litwiller, S.-H. Choi, I.J.J.o.M.S. Pinnau, Evaluation of sodium lignin sulfonate as draw solute in forward osmosis for desert restoration, J. Membr. Sci. 453 (2014) 463–470, https://doi.org/10.1016/j.memsci.2013.11.029.

[9] D. López-Carr, N.G. Pricope, K.M. Mwenda, G.A. Daldegan, A.J.S. Zvoleff, A conceptual approach towards improving monitoring of living conditions for populations affected by desertification, Land Degradation, and Drought, Sustainability 15 (2023) 9400, https://doi.org/10.3390/su15129400.

[10] R.C. Mainfort, W.L. Lawton, Laboratory Compaction Tests of Coarse-Graded Paving and Embankment Materials, Civil Aeronautics Administration, Technical Development and Evaluation Center, 1952.

[11] P.T. Sherwood, Soil stabilization by the use of chemical admixtures: a review of the present position, Road Research Lab Road Notes/UK (28) (1961).

[12] H. Wang, X. Sun, L. Miao, J. Zhang, W. Yin, L.J.A.G. Wu, Sand and dust storms control for sustainable anti-desertification: large-scale EICP-PVAc treatment field demonstration and insights, Acta Geotech. (2024) 1–19, https://doi.org/10.1007/s11440-024-02494-7.

[13] Q. Zhang, L. Fan, H. Wang, H. Han, Z. Zhu, X. Zhao, Y.J.P.S. Wang, E. Protection, A review of physical and chemical methods to improve the performance of water for dust reduction, Process. Saf. Environ. Prot. 166 (2022) 86–98, https://doi.org/10.1016/j.psep.2022.07.065.

[14] O.N.J.G. Maaitah, G. Engineering, Soil stabilization by chemical agent 30 (2012) 1345–1356.

[15] C.H. Hurley, T.H. Thornburn, Sodium Silicate Stabilization of Soils: A Review of the Literature, Soil Mechanics Laboratory, Department of Civil Engineering, Engineering …, 1971.

[16] M. Mali, N.C. Aery, Influence of silicon on growth, relative water contents and uptake of silicon, calcium and potassium in wheat grown in nutrient solution, J. Plant Nutr. 31 (2008) 1867–1876, https://doi.org/10.1080/01904160802402666.

[17] X. Zhou, Y. Shen, X. Fu, F.J.F.i.p.s., Wu, application of sodium silicate enhances cucumber resistance to fusarium wilt and alters soil microbial communities, Frontiers, Plant Sci. 9 (2018) 290362, https://doi.org/10.3389/fpls.2018.00624.

[18] D. Wang, Z. Wang, H. Wang, Feasibility and performance assessment of novel framework for soil stabilization using multiple industrial wastes, Constr. Build. Mater. 449 (2024) 138228, https://doi.org/10.1016/j.conbuildmat.2024.138228.

[19] S.T. Abdul-Hussein, M.H. Al-Furaiji, H. Meskher, D. Ghernaout, M. Fal, A. M. Alotaibi, Q.F. Alsalhy, Prospects of forward osmosis-based membranes for seawater mining: economic analysis, limitations and opportunities, Desalination 579 (2024) 117477, https://doi.org/10.1016/j.desal.2024.117477.

[20] Z. Li, R.V. Linares, M. Abu-Ghdaib, T. Zhan, V. Yangali-Quintanilla, G.J.W.R. Amy, Osmotically driven membrane process for the management of urban runoff in coastal regions, Water Res. 48 (2014) 200–209, https://doi.org/10.1016/j.watres.2013.09.028.

[21] I. Ibrar, S. Yadav, A. Altaee, A.K. Samal, J.L. Zhou, T.V. Nguyen, N.J.S.o.T.T.E., Ganbat, Treatment of biologically treated landfill leachate with forward osmosis: investigating membrane performance and cleaning protocols, Sci. Total Environ. 744 (2020) 140901, https://doi.org/10.1016/j.scitotenv.2020.140901.

[22] T.S. Chung, X. Li, R.C. Ong, Q. Ge, H. Wang, G. Han, Emerging forward osmosis (FO) technologies and challenges ahead for clean water and clean energy applications, Curr. Opin. Chem. Eng. 1 (2012) 246–257, https://doi.org/10.1016/j.coche.2012.07.004.

[23] S. Lee, C. Boo, M. Elimelech, S.J.J.o.m.s., Hong, Comparison of fouling behavior in forward osmosis (FO) and reverse osmosis (RO) 365 (2010) 34–39.

[24] N. Abounahia, I. Ibrar, T. Kazwini, A. Altaee, A.K. Samal, S.J. Zaidi, A.H. Hawari, Desalination by the forward osmosis: advancement and challenges, Sci. Total Environ. 886 (2023) 163901, https://doi.org/10.1016/j.scitotenv.2023.163901.

[25] D. Khanafer, I. Ibrahim, S. Yadav, A. Altaee, A. Hawari, J. Zhou, Brine reject dilution with treated wastewater for indirect desalination, J. Clean. Prod. 322 (2021) 129129, https://doi.org/10.1016/j.jclepro.2021.129129.

[26] F. Yang, X. Wang, Y. Shan, C. Wu, R. Zhou, N. Hengl, F. Pignon, Y. Jin, Pre-ozonation coupled with forward osmosis with fertilizer as draw solution for simultaneous wastewater treatment and agricultural irrigation, Desalination 592 (2024) 118187, https://doi.org/10.1016/j.desal.2024.118187.

[27] D. Li, X. Zhang, J. Yao, G.P. Simon, H.J.C.C. Wang, Stimuli-responsive polymer hydrogels as a new class of draw agent for forward osmosis desalination 47 (2011) 1710–1712.

[28] D. Li, X. Zhang, J. Yao, Y. Zeng, G.P. Simon, H.J.S.M. Wang, Composite polymer hydrogels as draw agents in forward osmosis and solar dewatering, Soft Matter 7 (2011) 10048–10056, https://doi.org/10.1039/C1SM06043K.

[29] X. Song, L. Wang, C.Y. Tang, Z. Wang, C. Gao, Fabrication of carbon nanotubes incorporated double-skinned thin film nanocomposite membranes for enhanced separation performance and antifouling capability in forward osmosis process, Desalination 369 (2015) 1–9, https://doi.org/10.1016/j.desal.2015.04.020.

[30] J. Garcia-Ivars, M.-I. Alcaina-Miranda, M.-I. Iborra-Clar, J.-A. Mendoza-Roca, L. Pastor-Alcañiz, Enhancement in hydrophilicity of different polymer phase-inversion ultrafiltration membranes by introducing PEG/Al2O3 nanoparticles, Sep. Purif. Technol. 128 (2014) 45–57, https://doi.org/10.1016/j.seppur.2014.03.012.

[31] Y. Tepe, C.E.J.N.A.J.o.A. Boyd, A sodium-nitrate-based, water-soluble, granular fertilizer for sport fish ponds, North American Journal of Aquaculture, 63 (2001) 328–332.doi:10.1577/1548-8454(2001)063<0328:ASNBWS>2.0.CO;2.

[32] D.N. KALBUADI, L.P. SANTI, D.H. GOENADI, J.J.M.P. BARUS, Application of bio-silicic acid to improve yield and fertilizer efficiency of paddy on tidal swamp land, Menara Perkebunan, 88 (2020).doi:10.22302/iribb.jur.mp.v88i2.378.

[33] >J. Kestin, H.E. Khalifa, R.J.J.J.P.C.R.D. Correics, Tables of the dynamic and kinematic viscosity of aqueous NaCl solutions in the temperature range 20-150 “C cand the pressure range 0.1-35 MPa, J. Phys. Chem. Ref. Data Monogr., 10 (1981),.

[34] K. Xue, S.S. Liow, A.A. Karim, Z. Li, X.J. Loh, A recent perspective on noncovalently formed polymeric hydrogels, Chem. Rec. 18 (2018) 1517–1529, https://doi.org/10.1002/tcr.201800015.

[35] P.F. McMillan, B.J.B.d.M. Piriou, Raman spectroscopic studies of silicate and related glass structure: a review 106 (1983) 57–75.

[36] J.C. McRae, M.A. Smith, B.P. Duncan, E. Holihan, V. Liberman, C. Rock, D. Beck, L. M.J.I.T.o.C. Racz, Packaging, M. Technology, Sodium Metasilicate-Based Inorganic Composite for Heterogeneous Integration of Microsystems, 11 (2020) 144–152,.

[37] M. Besbes, N. Fakhfakh, M. Benzina, Characterization of silica gel prepared by using sol–gel process, Phys. Procedia 2 (2009) 1087–1095, https://doi.org/10.1016/j.phpro.2009.11.067.

[38] M. Kahrizi, R.R. Gonzales, L. Kong, H. Matsuyama, P. Lu, J. Lin, S. Zhao, Significant roles of substrate properties in forward osmosis membrane performance: A review, Desalination 528 (2022) 115615, https://doi.org/10.1016/j.desal.2022.115615.

[39] S.N.A. Idris, N.J.M.T.P. Jullok, Evaluation of commercial reverse osmosis and forward osmosis membranes at different draw solution concentration in pressure retarded osmosis process 46 (2021) 2065–2069.

[40] Y. Aedan, A. Altaee, J. Zhou, H.K. Shon, Perfluorooctanoic acid-contaminated wastewater treatment by forward osmosis, Performance analysis 934 (2024) 173368.

[41] I. Ibrar, S. Yadav, A. Altaee, A. Hawari, V. Nguyen, J. Zhou, A novel empirical method for predicting concentration polarization in forward osmosis for single and

multicomponent draw solutions, Desalination 494 (2020) 114668, https://doi.org/10.1016/j.desal.2020.114668.
[42] C.R. Bartels, K.J.D. Andes, W. Treatment, Consideration of energy savings in SWRO, Desalin. Water Treat. 51 (2013) 717–725, https://doi.org/10.1080/19443994.2012.700038.
[43] B. Mayor, Growth patterns in mature desalination technologies and analogies with the energy field, Desalination 457 (2019) 75–84, https://doi.org/10.1016/j.desal.2019.01.029.
[44] I. Ibrar, S. Yadav, A. Altaee, J. Safaei, A.K. Samal, S. Subbiah, G. Millar, P. Deka, J. J.C. Zhou, Sodium docusate as a cleaning agent for forward osmosis membranes fouled by landfill leachate wastewater, Chemosphere 308 (2022) 136237, https://doi.org/10.1016/j.chemosphere.2022.136237.